Inorganic Chemistry

including bioinorganic chemistry

August 19, 2013
Volume 52, Number 16
pubs.acs.org/IC

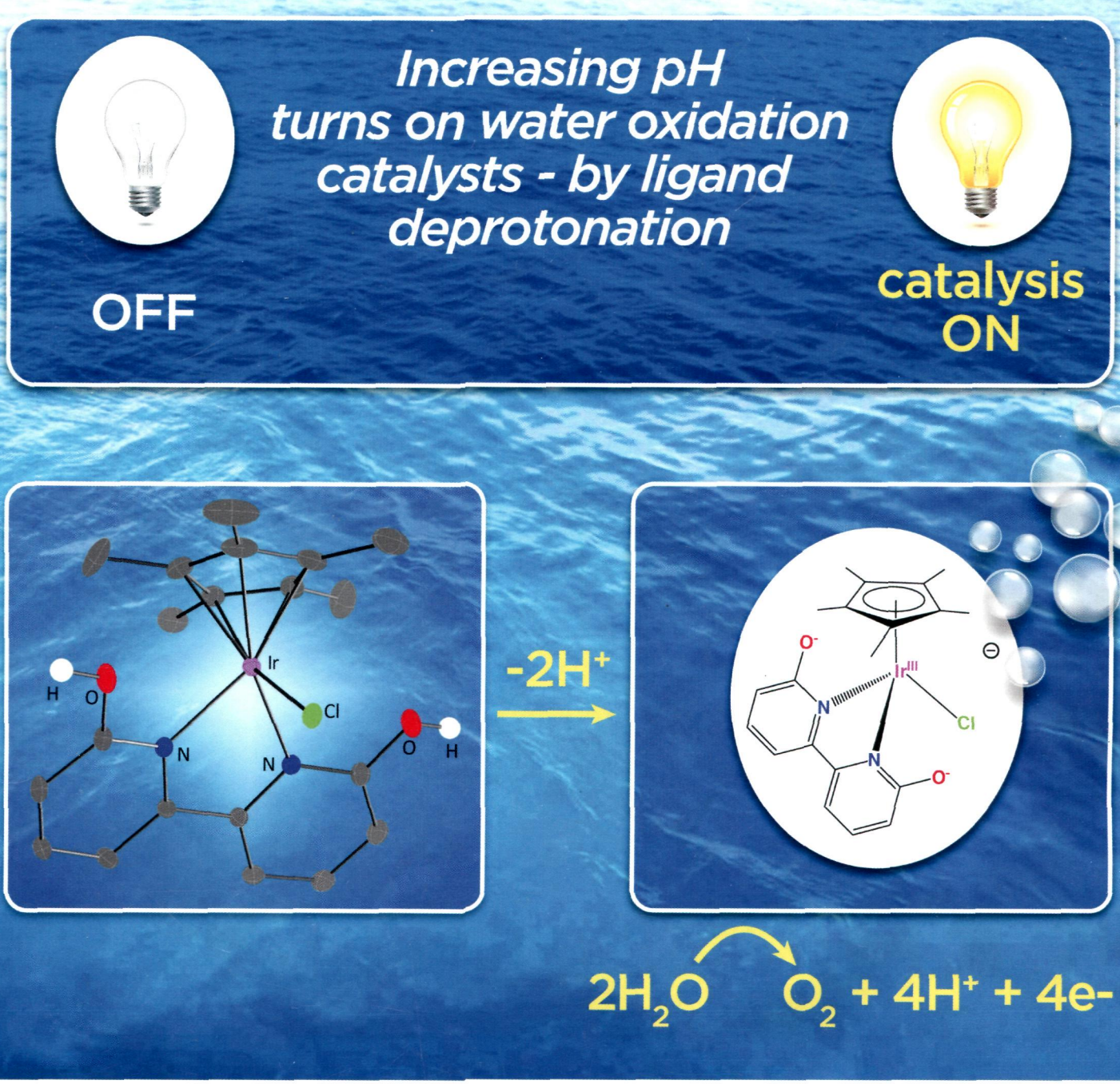

ACS Publications
MOST TRUSTED. MOST CITED. MOST READ.

www.acs.org

Inorganic Chemistry

AUGUST 19, 2013
VOLUME 52 ISSUE 16

INOCAJ 52(16) 9163–9698 (2013)
ISSN 0020-1669

ON THE COVER: Changing the pH of water can activate homogeneous water oxidation catalysts by ligand deprotonation. Dianionic X_2 ligands are known to enhance water oxidation by facilitating catalyst oxidation, but the use of ligands that change from L_2 to X_2 in situ is novel and here leads to switchable catalyst properties. For more details, see J. DePasquale, I. Nieto, L. E. Reuther, C. J. Herbst-Gervasoni, J. J. Paul, V. Mochalin, M. Zeller, C. M. Thomas, A. W. Addison, and E. T. Papish, p 9175.

Communications

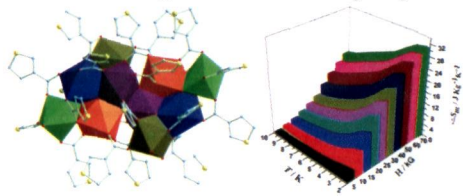

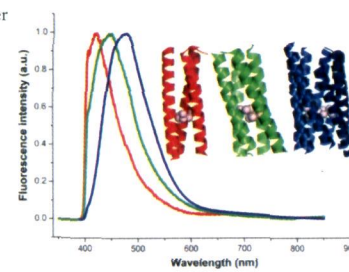

9169 S dx.doi.org/10.1021/ic401329d

Structural Assembly from Phosphate to Germanophosphate by Applying Germanate as a Binder

Ya-Xi Huang,* Biao Liu, Lei Wen, Xin Zhang, Wei Sun, Jun Lin, Chun-Zuo Huang, Rong-Chuan Zhuang, Jin-Xiao Mi, and Jing-Tai Zhao

Structural assembly from layers of transition-metal phosphate to germanophosphate frameworks by applying GeO_6 octahedral chains as binders. The Jahn−Teller effect makes an iron compound with undulated layers and a cadmium compound with flat layers, resulting in different shapes of 12-ring channels and quite different powder X-ray diffraction patterns.

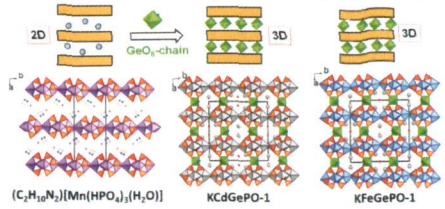

9172 S dx.doi.org/10.1021/ic401690s

Mixed-Valence Uranium(V,VI) and Uranyl Oxyhydroxides Synthesized under High-Temperature, High-Pressure Hydrothermal Conditions: $Na_5[U_5O_{16}(OH)_2]$ and $Na_5[U_5O_{17}(OH)]$

Hsin-Kuang Liu and Kwang-Hwa Lii*

An unusual mixed-valence uranium oxyhydroxide with a sheet structure was synthesized with zinc metal as the reducing agent under high-temperature, high-pressure hydrothermal conditions. The sheet anion topology of the structure is the same as that of the uranyl mineral sayrite, but the squares are populated by $U^V(OH)_2^{3+}$ ions. The valence state of uranium was confirmed by X-ray photoelectron spectroscopy. A uranyl oxyhydroxide with a new sheet anion topology was also synthesized.

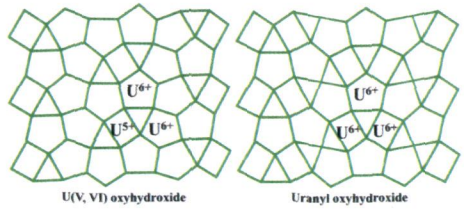

Articles

9175 S dx.doi.org/10.1021/ic302448d

Iridium Dihydroxybipyridine Complexes Show That Ligand Deprotonation Dramatically Speeds Rates of Catalytic Water Oxidation

Joseph DePasquale, Ismael Nieto, Lauren E. Reuther, Corey J. Herbst-Gervasoni, Jared J. Paul,* Vadym Mochalin, Matthias Zeller, Christine M. Thomas, Anthony W. Addison, and Elizabeth T. Papish*

Iridium complexes of dihydroxybipyridine are switchable precatalysts for water oxidation. They become more highly active at higher pH values because of ligand deprotonation. This appears to be the first example of using pH as a switch to activate water oxidation catalysts, and in effect these dhbp ligands are converted from L2 to X2 type ligands in situ, thereby facilitating oxidation events.

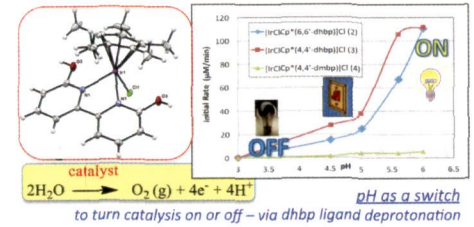

9184 S dx.doi.org/10.1021/ic4001818

Highly Uniform α-$NaYF_4$:Yb/Er Hollow Microspheres and Their Application as Drug Carrier

Yunhua Han, Shili Gai,* Ping'an Ma, Liuzhen Wang, Milin Zhang, Shaohua Huang, and Piaoping Yang

Uniform α-$NaYF_4$:Yb/Er hollow microspheres were first fabricated by a two-step hydrothermal method. Under 980 nm IR laser excitation, the α-$NaYF_4$:Yb/Er hollow spheres can exhibit bright UC luminescence. This sample exhibits sustained and pH-dependent release properties, and the sample has high potential to be tracked or monitored by the change of upconversion emission intensity.

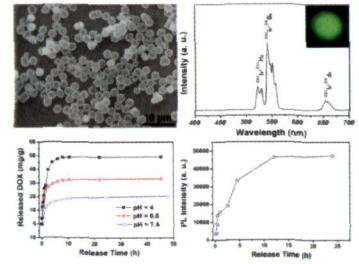

9192 (S) dx.doi.org/10.1021/ic400089s

Design of Medium Band Gap Ag–Bi–Nb–O and Ag–Bi–Ta–O Semiconductors for Driving Direct Water Splitting with Visible Light

Limin Wang, Bingfei Cao, Wei Kang, Mark Hybertsen, Kazuhiko Maeda, Kazunari Domen, and Peter G. Khalifah*

The synthesis, structure, and characterization is reported for two pyrochlore-family direct band gap semiconductors that are well suited for harvesting visible light for solar water splitting applications, $AgBiNb_2O_7$ ($E_g \approx 2.72$ eV) and $Ag_{4/5}Bi_{5/6}Ta_2O_{6.65}$ ($E_g \approx 2.96$ eV). $AgBiNb_2O_7$ has both improved light absorption characteristics and better placed energy levels for driving overall water splitting than the classic semiconductor WO_3.

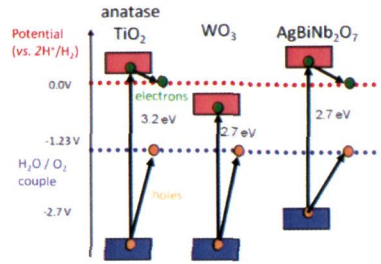

9206 (S) dx.doi.org/10.1021/ic4002048

Absorption and Electrochemical Properties of Cobalt and Iron Phthalocyanines and Their Quaternized Derivatives: *Aggregation Equilibrium and Oxygen Reduction Electrocatalysis*

Thiago Teixeira Tasso, Taniyuki Furuyama, and Nagao Kobayashi*

The synthesis, aggregation, and electronic properties of Co(II) and Fe(II) phthalocyanines (Pcs) are reported. The quaternized compounds showed increased water solubility. The catalytic effect of Pcs in the oxygen reduction reaction (ORR) was also investigated.

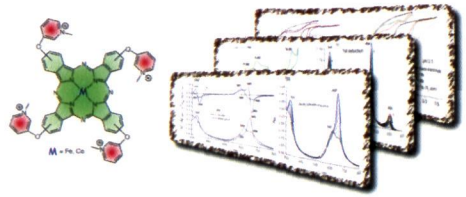

9216 (S) dx.doi.org/10.1021/ic400292g

Mixed-Valent Dicobalt and Iron–Cobalt Complexes with High-Spin Configurations and Short Metal–Metal Bonds

Christopher M. Zall, Laura J. Clouston, Victor G. Young Jr., Keying Ding, Hyun Jung Kim, Danylo Zherebetskyy, Yu-Sheng Chen, Eckhard Bill,* Laura Gagliardi,* and Connie C. Lu*

Cobalt–cobalt and iron–cobalt bonds are investigated in coordination complexes with formally mixed-valent $[M_2]^{3+}$ cores. Their solid-state structures reveal short metal–metal bond distances of 2.29 Å for Co–Co and 2.18 Å for Fe–Co. The dicobalt and iron–cobalt complexes are high-spin, and spectroscopic and theoretical data suggest that the $[Co_2]^{3+}$ and $[FeCo]^{3+}$ cores, respectively, are delocalized.

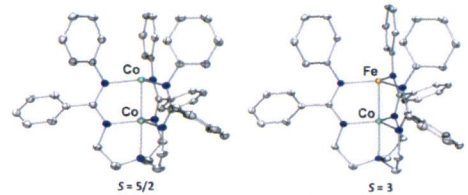

9229 (S) dx.doi.org/10.1021/ic4004033

Assessing the Impact of Electronic and Steric Tuning of the Ligand in the Spin State and Catalytic Oxidation Ability of the Fe^{II}(Pytacn) Family of Complexes

Irene Prat, Anna Company,* Teresa Corona, Teodor Parella, Xavi Ribas, and Miquel Costas*

A family of iron complexes with the general formula $[Fe^{II}(^{R,R'}Pytacn)(X)_2]^{n+}$ is described. Herein, we study the influence of R and R′ on the electronic properties of the coordinated iron center using X-ray diffraction, ^1H NMR spectroscopy, UV–vis spectroscopy, and magnetic susceptibility measurements. Isotopic labeling studies in the epoxidation and *cis*-dihydroxylation reactions show that R has a definitive role in dictating the origin of the oxygen atom that is transferred in the epoxidation reaction.

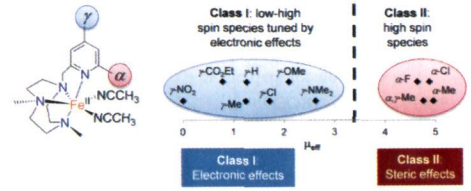

9245 (S) dx.doi.org/10.1021/ic4004356

Substituent Effects on the Biological Properties of Zn-Salophen Complexes

Ilaria Giannicchi, Rosa Brissos, David Ramos, Joaquin de Lapuente, João Carlos Lima, Antonella Dalla Cort,* and Laura Rodríguez*

The biological activity of three luminescent 5,5′-X-substituted Zn-salophen complexes (X = OCH3, Br, and NO2) has been analyzed. The strongest interaction with free plasmid DNA is observed for the 5,5′-dinitro-substituted Zn-salophen complex. Cellular uptake and cytotoxicity studies undertaken with these metal complexes show that they enter the cells but are not cytotoxic.

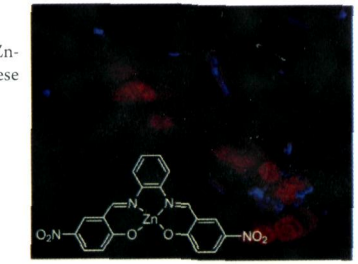

9254 (S) dx.doi.org/10.1021/ic400491q

Photophysical Properties of Endohedral Amine-Functionalized Bis(phosphine) Pt(II) Complexes as Models for Emissive Metallacycles

J. Bryant Pollock,* Timothy R. Cook, Gregory L. Schneider, Daniel A. Lutterman, Andrew S. Davies, and Peter J. Stang*

Endohedral amine-functionalized supramolecular coordination complexes (SCCs) synthesized from 2,6-bis(pyrid-3-ylethynyl) aniline and 2,6-bis(pyrid-4-ylethynyl) aniline vary significantly despite differing only in the position of the coordinating nitrogen. Steady-state absorption and emission and excited-state lifetime measurements were performed on a series of coordination complexes to probe this system. Density functional theory (DFT) and time-dependent DFT (TD-DFT) calculations were performed to provide insight into the character of the observed optical transitions.

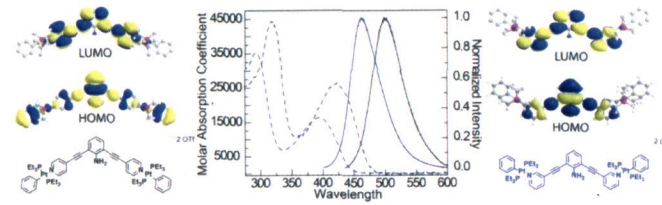

9266 S dx.doi.org/10.1021/ic4004559

Tuning the Photophysical Properties of *anti*-$B_{18}H_{22}$: Efficient Intersystem Crossing between Excited Singlet and Triplet States in New 4,4′-$(HS)_2$-*anti*-$B_{18}H_{20}$.

Vicenta Sauri, Josep M. Oliva,* Drahomír Hnyk, Jonathan Bould, Jakub Braborec, Manuela Merchán, Pavel Kubát, Ivana Císařová, Kamil Lang,* and Michael G. S. Londesborough*

The tuning of the photophysical properties of the highly fluorescent boron hydride cluster *anti*-$B_{18}H_{22}$ (**1**), by straightforward chemical substitution to produce 4,4′-$(HS)_2$-*anti*-$B_{18}H_{20}$ (**2**), facilitates intersystem crossing from excited singlet states to a triplet manifold. This subsequently enhances $O_2(^1\Delta_g)$ singlet oxygen production from a quantum yield of $\Phi_\Delta \sim 0.008$ in **1** to 0.59 in **2**.

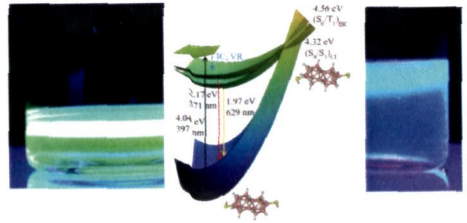

9275 S dx.doi.org/10.1021/ic400509q

Synthesis, Structure, and Optical and Redox Properties of Chlorophyll Derivatives Directly Coordinating Ruthenium Bisbipyridine at the Peripheral β-Diketonate Moiety.

Yusuke Kinoshita, Youhei Yamamoto, and Hitoshi Tamiaki*

We synthesized the sires of ruthenium bisbipyridine complexes directly coordinated with the diketonate moiety at the C3 position of chlorophyll derivatives. Electronic absorption spectra of chlorin–ruthenium conjugates showed the MLCT band derived from the ruthenium bipyridine moiety around 500 nm, in addition to absorption bands characteristic of a chlorophyll moiety. The ruthenium coordination induced small shifts in redox potentials of the chlorophyll moiety, but it suppressed its fluorescence emission by the internal heavy atom effect.

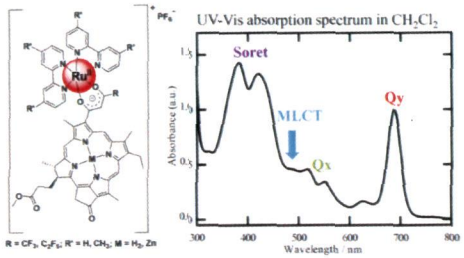

9284 S dx.doi.org/10.1021/ic400542x

Exploring the Assembly of Supramolecular Polyoxometalate Triangular Morphologies with Johnson Solid Cores: $[(Mn^{II}(H_2O)_3)_2(K\subset\{\alpha\text{-}GeW_{10}Mn^{II}_2O_{38}\}_3)]^{19-}$

Pedro I. Molina, Haralampos N. Miras, De-Liang Long, and Leroy Cronin*

A new member of the "trinity" POM family with a core with Johnson solid geometry and D_{3d} symmetry is reported. The interplay of the ionic radius of the alkali metals and the solution's ionic strength allowed us to direct the assembly toward the formation of a new supramolecular species with triangular morphology and control the cavity size associated with specific symmetry and geometrical features.

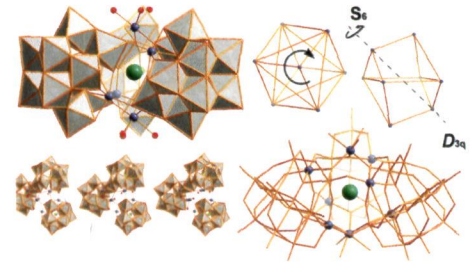

9290 S dx.doi.org/10.1021/ic400577v

***Structural Factors That Enhance Lithium Mobility in Fast-Ion $Li_{1+x}Ti_{2-x}Al_x(PO_4)_3$ ($0 \le x \le 0.4$) Conductors Investigated by* Neutron Diffraction in the Temperature Range 100–500 K**

K. Arbi, M. Hoelzel, A. Kuhn, F. García-Alvarado, and J. Sanz*

Structural features responsible for lithium conductivity of the $Li_{1+x}Ti_{2-x}Al_x(PO_4)_3$ series (x = 0, 0.2, and 0.4) have been deduced by Rietveld analysis of neutron diffraction (ND) patterns recorded in the temperature range 100–500 K. Analysis of the Fourier map differences showed that Li ions occupy M1 sites at ternary axes and, to a lower extent, M3 sites disposed near M2 sites. The information deduced by ND is compared with that deduced previously by NMR and impedance spectroscopy. The existence of two lithium motion regimes has been related to variation of the lithium and oxygen thermal factors.

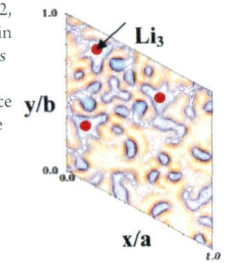

9297 S dx.doi.org/10.1021/ic400746n

Synthesis, Spectroscopic Properties, and Photoinduced CO-Release Studies of Functionalized Ruthenium(II) Polypyridyl Complexes: Versatile Building Blocks for Development of CORM–Peptide Nucleic Acid Bioconjugates

Caroline Bischof, Tanmaya Joshi, Aakanksha Dimri, Leone Spiccia, and Ulrich Schatzschneider*

Ruthenium(II) dicarbonyl complexes of formula $[RuCl_2(CO)_2(N\text{–}N)]$ were synthesized and evaluated as photoactivatable CO-releasing molecules (PhotoCORMs). Some of the compounds were stable under physiological conditions in the dark for up to 15 h, establishing them as CO prodrugs, while illumination at 365 nm lead to CO transfer to myoglobin. Conjugation of one of the title compounds to a peptide nucleic acid (PNA) building block opens the way for a targeted delivery of CO to biological systems.

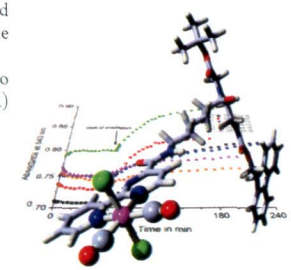

9309 S dx.doi.org/10.1021/ic400751n

A Trigonal Prismatic Ligand in the Metal-Mediated Self-Assembly of One- and Two-Dimensional Metallosupramolecular Polymers

Wen-Jing Hu, Long-Qing Liu, Ming-Liang Ma,* Xiao-Li Zhao, Yahu A. Liu, Xian-Qiang Mi, Biao Jiang,* and Ke Wen*

A prismatic bicycooxacalixaromatic ligand **L** was synthesized and used in the study of metal-mediated self-assembly. Various sized metallomacrocyclic units are presented in the resulting metallosupramolecular polymers for hosting neutral and charged guest species.

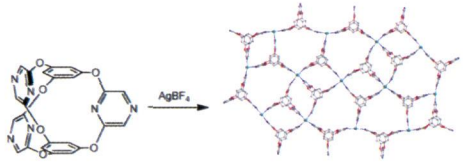

9320 S dx.doi.org/10.1021/ic4008334

Porous Ionic Crystals Modified by Post-Synthesis of $K_2[Cr_3O(OOCH)_6(etpy)_3]_2[\alpha\text{-}SiW_{12}O_{40}]\cdot 8H_2O$ through Single-Crystal-to-Single-Crystal Transformation

Sayaka Uchida, Eri Takahashi, and Noritaka Mizuno*

A porous ionic crystal of $K_2[Cr_3O(OOCH)_6(etpy)_3]_2[\alpha\text{-}SiW_{12}O_{40}]\cdot 8H_2O$ (etpy = 4-ethylpyridine) was modified by post-synthetic methods. Post-synthesis modification proceeded via two steps (acid treatment followed by ion-exchange) in an aqueous solution and a single-crystal-to-single-crystal manner. Increase in sorption capacity by the two-step post-synthesis modification was confirmed by vapor sorption isotherms and Monte Carlo-based simulations using water as a probe molecule. The role of K^+ ions as water binding sites was confirmed by water sorption isotherms of alkali metal ion-exchanged compounds.

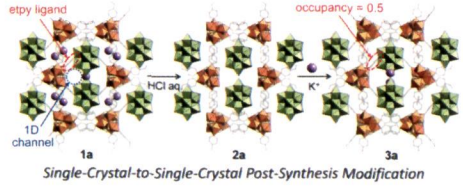

Single-Crystal-to-Single-Crystal Post-Synthesis Modification

9327 S dx.doi.org/10.1021/ic400829d

Aryl-Linked Salicylaldoxime-Based Copper(II) Helicates and "Boxes": Synthesis, X-ray Analysis, and Anion Influence on Complex Structure

Ajay Pal Singh Pannu, James R. Stevens, and Paul G. Plieger*

The synthesis and spectroscopic analysis of both "metal-only" and anion encapsulated salicylaldoxime-based complexes utilizing a new 1,3-xylyl strap are described. X-ray crystallographic analysis reveals that the aromatic spacer restricts the confirmation flexibility of the resulting complexes leading to dicopper(II) double helicate and dicopper(II) 2 + 2 "box" structural forms.

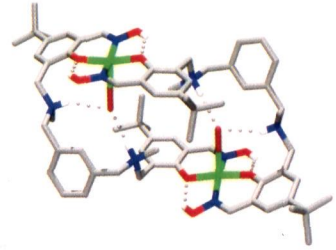

9338 S dx.doi.org/10.1021/ic4009009

Origin of Small Barriers in Jahn–Teller Systems: Quantifying the Role of 3d–4s Hybridization in the Model System NaCl:Ni^+

M. T. Barriuso,* B. Ortiz-Sevilla, J. A. Aramburu, P. García-Fernández, J. M. García-Lastra, and M. Moreno

Seeking to clear up the microscopic origin of the energy barrier, B, of Jahn–Teller (JT) systems both periodic and cluster ab initio calculations on the model system NaCl:Ni^+ have been carried out. It is quantitatively proven that the elongated geometry observed for NaCl:Ni^+ is due to the 3d–4s vibronic admixture, which is slightly larger than the anharmonicity in the e_g JT mode that favors a compressed geometry. All calculations performed on the model system lead, in fact, to values $|B| \leq 20$ meV, certainly smaller than $B = 500$ cm^{-1} derived for NaCl:M^{2+} (M = Ag, Rh) or $B = 1024$ cm^{-1} obtained for KCl:Ag^{2+}. As a main conclusion, the barrier in JT systems cannot be understood, neglecting the tiny changes of the electronic density involved in small distortions.

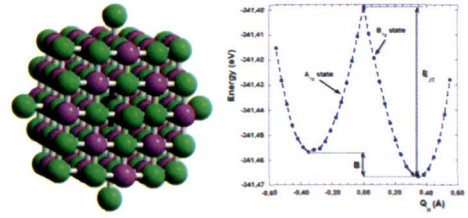

9349 S dx.doi.org/10.1021/ic400918d

Expected and Unexpected Transformations of Manganese(III) Tris(4-nitrophenyl)corrole

Pinky Singh, Gargi Dutta, Israel Goldberg, Atif Mahammed, and Zeev Gross*

Oxidative amination of manganese(III) corrole leads to (nitrido)manganese(V) azahemiporphycenes.

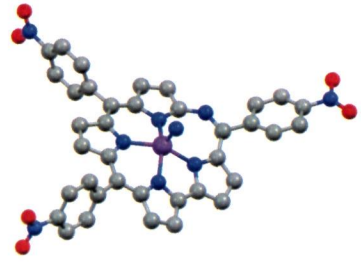

9356 S dx.doi.org/10.1021/ic400927m

First-Principles Study of Microporous Magnets M-MOF-74 (M = Ni, Co, Fe, Mn): the Role of Metal Centers

Qiuju Zhang, Baihai Li, and Liang Chen*

The spin-polarized total density of states and spin density for ferromagnetic Fe-MOF-74 are given. The inset is the high-spin state of Fe^{II} $3d^6$.

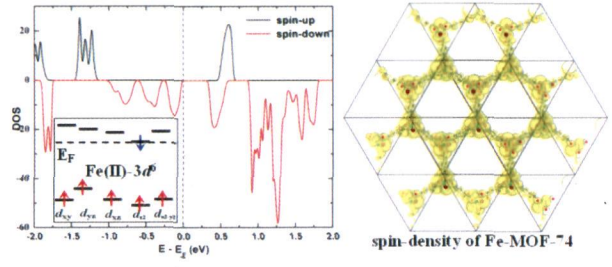

9363 S dx.doi.org/10.1021/ic400932m

Visible Light Water Oxidation Using a Co-Catalyst Loaded Anatase-Structured $Ti_{1-(5x/4)}Nb_xO_{2-y-\delta}N_y$ Compound

Tanya M. Breault, James J. Brancho, Ping Guo, and Bart M. Bartlett*

TiO_2:(Nb,N)-25, our moniker for anatase-structured $Ti_{1-(5x/4)}Nb_xO_{2-y-\delta}N_y$ ($x = 0.25$, $y = 0.02$), is a photocatalyst for water oxidation with concomitant IO_3^- reduction when loaded with 1 wt % RuO_2. The material is catalytically active using solar wavelengths, determined by using a series of cut-on filters and by gas-phase mass spectrometry analysis of a $H_2{}^{18}O$ labeling study.

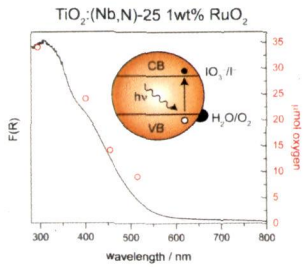

9369 S dx.doi.org/10.1021/ic400945u

New Media for Classical Coordination Chemistry: Phase Transfer of Werner and Related Polycations into Highly Nonpolar Fluorous Solvents

Subrata K. Ghosh, Ann Sullivan Ojeda, Juan Guerrero-Leal, Nattamai Bhuvanesh, and John A. Gladysz*

An improved scalable synthesis of $NaB(3,5\text{-}C_6H_3(R_{f6})_2)_4$ (R_{f6} = perfluorohexyl), a sodium salt of a highly fluorophilic anion, is reported. This anion renders the tri- and dications $[Co(en)_3]^{3+}$, $[Co(R,R\text{-chxn})_3]^{3+}$ (chxn = 1,2-cyclohexanediamine) and $[Ru(bipy)_3]^{2+}$ highly soluble in fluorous solvents, with toluene/perfluoro(methylcyclohexane) partition coefficients of $\leq 1{:}\geq 99$.

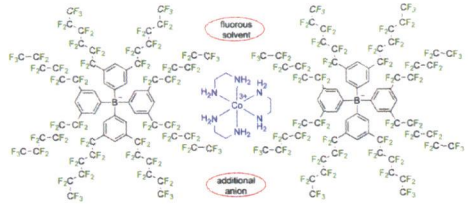

9379 S dx.doi.org/10.1021/ic400953e

Single-Ion Magnetic Anisotropy and Isotropic Magnetic Couplings in the Metal–Organic Framework Fe_2(dobdc)

Rémi Maurice, Pragya Verma, Joseph M. Zadrozny, Sijie Luo, Joshua Borycz, Jeffrey R. Long,* Donald G. Truhlar,* and Laura Gagliardi*

The magnitude of the main magnetic interactions in the metal–organic framework Fe_2(dobdc) are assessed with quantum chemical calculations performed on a finite cluster. It is shown that the axial single-ion anisotropy parameter value is of the same order of magnitude as the nearest neighbor isotropic couplings, qualifying the system as belonging to the weak-exchange regime. Additional magnetic data reveal a metamagnetic behavior at low temperature, attributable to various microscopic interactions.

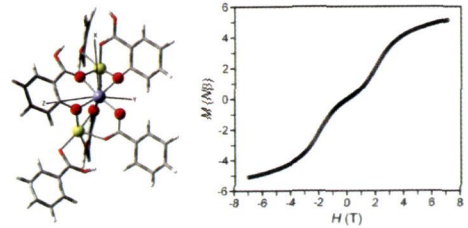

9390 S dx.doi.org/10.1021/ic4009569

Basis for Sensitive and Selective Time-Delayed Luminescence Detection of Hydroxyl Radical by Lanthanide Complexes

Katie L. Peterson, Maximilian J. Margherio, Phi Doan, Kyle T. Wilke, and Valérie C. Pierre*

The design, evaluation and mechanism of action of molecular probes for the detection of hydroxyl radical (HO•) by time-delayed luminescence spectroscopy directly in water at neutral pH with high sensitivity and selectivity over competing ROS and RNS are presented. These bimolecular probes consist of an aromatic acid that reacts with HO• to produce hydroxylated chromophores that readily bind to Tb-DO3A and sensitize lanthanide-centered emission.

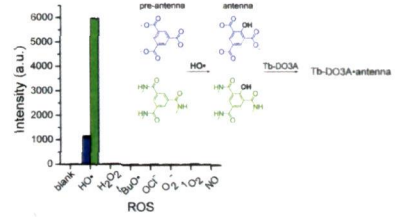

9399 S dx.doi.org/10.1021/ic4009653

β-Mn-Type $Co_{8+x}Zn_{12-x}$ as a Defect Cubic Laves Phase: Site Preferences, Magnetism, and Electronic Structure

Weiwei Xie, Srinivasa Thimmaiah, Jagat Lamsal, Jing Liu, Thomas W. Heitmann, Dante Quirinale, Alan I. Goldman, Vitalij Pecharsky, and Gordon J. Miller*

Structural, magnetic, and bonding studies of β-Mn-type $Co_{8+x}Zn_{12-x}$ phases reveal clear atomic site preferences, ferromagnetism associated with local moments at Co atoms, and structural relationships with a specific ordered vacancy model of the cubic Laves phase.

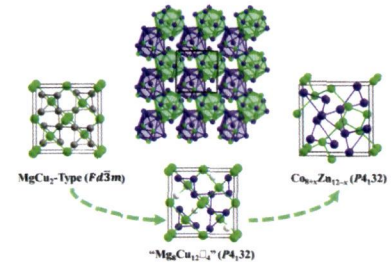

9409 S dx.doi.org/10.1021/ic400980b

Zero-Field Splitting in Pseudotetrahedral Co(II) Complexes: a Magnetic, High-Frequency and -Field EPR, and Computational Study

Monika Idešicová, Ján Titiš,* J. Krzystek,* and Roman Boča

The zero-field splitting of a series of mononuclear pseudotetrahedral Co(II) complexes with heterocyclic N-donor ligands was determined to a high precision and accuracy using SQUID magnetometry and HFEPR spectroscopy. *Ab initio* quantum chemical calculations have been used to obtain correlations between the geometric and electronic structure and magnetic properties.

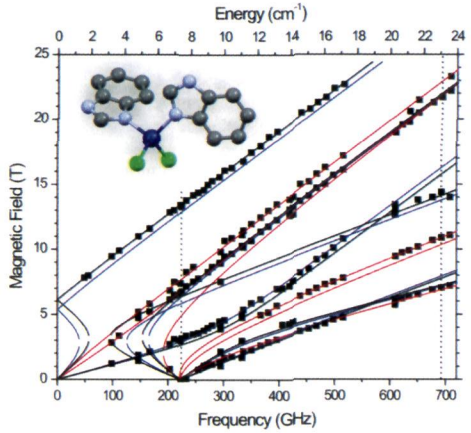

9418 S dx.doi.org/10.1021/ic400989v

Cyclodextrin Capped Gold Nanoparticles as a Delivery Vehicle for a Prodrug of Cisplatin

Yi Shi, Jerry Goodisman, and James C. Dabrowiak*

The synthesis, characterization, and cytotoxic properties of a gold nanoparticle having surface bound β-cyclodextrin capable of accepting an adamantane conjugated Pt(IV) complex through a host–guest interaction are described. The work demonstrates the feasibility of using a two-component modular assembly approach for producing a polyfunctional nanodrug.

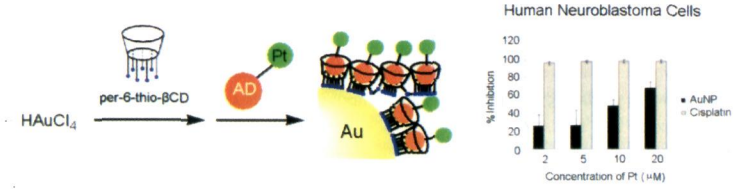

9427 S dx.doi.org/10.1021/ic401008y

Toward the Understanding of Radical Reactions: Experimental and Computational Studies of Titanium(III) Diamine Bis(phenolate) Complexes

Sónia Barroso, Filipe Madeira, Maria José Calhorda, M. João Ferreira, M. Teresa Duarte, and Ana M. Martins*

The reactivity of paramagnetic titanium(III) species is described. The results revealed that these species are very reactive and sensitive to the experimental conditions. Cationic Ti(IV) complexes tend to balance their extreme acidity by abstracting X type ligands or oxygen from the medium. Along with these rearrangements, the ancillary ligand may display hemilabile behavior.

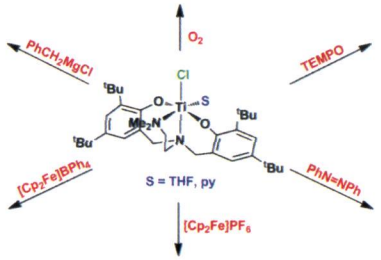

9440 S dx.doi.org/10.1021/ic4010664

Tris(2-pyridylborate) (Tpyb) Metal Complexes: Synthesis, Characterization, and Formation of Extrinsically Porous Materials with Large Cylindrical Channels

Chengzhong Cui, Patrick R. Shipman, Roger A. Lalancette,* and Frieder Jäkle*

A series of metal complexes $(Tpyb)_2M$ (M = Mg, Fe, Mn) based on the scorpionate-like *t*-butylphenyltris(2-pyridyl)borate ligand have been synthesized. Characterization by single crystal X-ray diffraction revealed the unexpected formation of large (up to ca. 8 Å diameter) channels propagating throughout the crystal lattice. The solvent in the large hexagonal pores of $(Tpyb)_2Mg$ was readily removed under high vacuum, and surface area and gas uptake measurements further confirmed the permanent porosity.

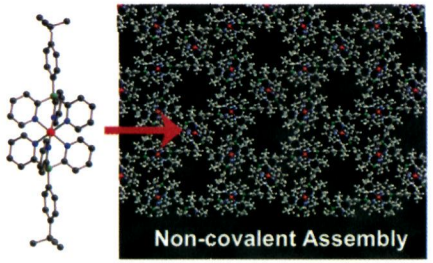

9449 S dx.doi.org/10.1021/ic401068n

Hierarchical MnO_2/SnO_2 Heterostructures for a Novel Free-Standing Ternary Thermite Membrane

Yong Yang, Zhi-Cheng Zhang, Peng-Peng Wang, Jing-Chao Zhang, Farhat Nosheen, Jing Zhuang, and Xun Wang*

MnO_2/SnO_2 heterostructures were obtained via a surfactant-free hydrothermal method. The secondary growth SnO_2 relies on the minimization of surface energy and interfacial lattice mismatch. A bottom-up method was presented to produce nanoenergetic composites by assembling nanoaluminum and MnO_2/SnO_2 hierarchical nanostructures into a free-standing ternary thermite membrane.

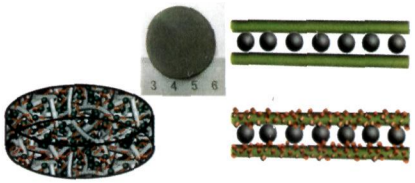

9456 S dx.doi.org/10.1021/ic401105v

Spontaneous Formation in the Dark, and Visible Light-Induced Cleavage, of a Ru–S Bond in Water: A Thermodynamic and Kinetic Study

Azadeh Bahreman, Bart Limburg, Maxime A. Siegler, Elisabeth Bouwman, and Sylvestre Bonnet*

The thermal and photochemical conversion between $[Ru(tpy)(N{-}N)(H_2O)]^{2+}$ and $[Ru(tpy)(N{-}N)(Hmte)]^{2+}$ is studied, in water, for four bidentate chelates N–N. According to variable-temperature kinetic measurements the dark substitution of water by Hmte shifts from an interchange associative mechanism with the least hindered chelate (bpy) to an interchange dissociative mechanism with the most hindered one (dmbpy). In the two intermediate systems (biq, dcbpy) the Ru–S bond forms spontaneously in the dark but is selectively broken by visible light irradiation.

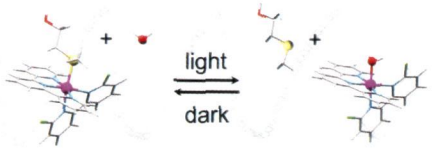

9470 S dx.doi.org/10.1021/ic401125e

Mo- and W-Based Organic Nanostructures Prepared from Bulk Crystal Isomorphs Consisted of $[(CH_3CH_2)_3NH)]_2[MO_2(C_{14}H_6O_4)_2]$ (M = Mo, W)

B. Zhang, S. Z. Du, X. M. Lu, G. Wang, and J. Fen*

Two new crystal isomorphs consisting of complexes $[(CH_3CH_2)_3NH)]_2[MoO_2(C_{14}H_6O_4)_2]$ (**1**) and $[(CH_3CH_2)_3NH)]_2[WO_2(C_{14}H_6O_4)_2]$ (**2**) have been synthesized, respectively, and from which Mo-based flexible and durable nanopipes and W-based rigid and fragile nanotubules have been prepared separately, which revealed that the change of the metal in the coordination center of the isomorphs can result in obvious variation to their nanostructures.

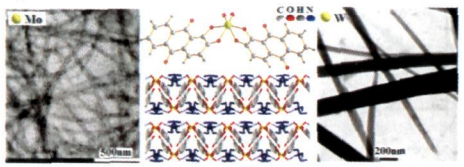

9479 S dx.doi.org/10.1021/ic4011345

Synthesis and Structural Characterization of Base-Stabilized Oligomeric Heterovinylidenes

Wing-Por Leung,* Wang-Kin Chiu, and Thomas C. W. Mak

The reaction of the monolithium salt $[Li\{CH(PPh_2)(PPh_2{=}NSiMe_3)\}(THF)_2]$ (**2**) with $GeCl_2{\cdot}$1,4-dioxane has led to the formation of a germavinylene moiety, which trimerized to form a new heterocyclic cage compound, $[\{(PPh_2{=}NSiMe_3)(PPh_2)C{=}Ge{:}\}\{(PPh_2{=}NSiMe_3)(PPh_2)C\}_2Ge{\rightarrow}Ge{:}]$ (**3**). A similar reaction of the lithium methanide complex **2** with $SnCl_2$ afforded the stannavinylidene moiety, which underwent a "head-to-tail" cycloaddition to form a stable 1,3-distannacyclobutane, **4**. A trapping reaction of **4** with diiron nonacarbonyl gave the novel iron stannavinylidene complex **5**.

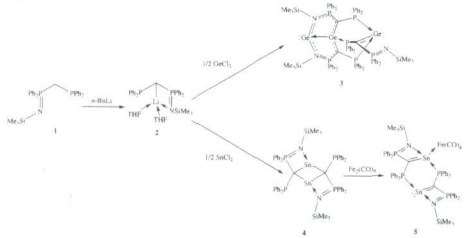

9487 S dx.doi.org/10.1021/ic401143g

Series of Uranyl-4,4′-biphenyldicarboxylates and an Occurrence of a Cation–Cation Interaction: Hydrothermal Synthesis and in Situ Raman Studies

Paula M. Cantos, Laurent J. Jouffret, Richard E. Wilson, Peter C. Burns, and Christopher L. Cahill*

The hydrothermal syntheses and crystal structures of three uranyl-4,4′-biphenyldicarboxylate hybrid materials have been reported: $(UO_2)(C_{14}O_4H_8)$ (**1**); $[(UO_2)_2(C_{14}O_4H_8)_2(OH)]{\cdot}(NH_4)(H_2O)$ (**2**); $(UO_2)_2(C_{14}O_4H_8)(OH)_2$ (**3**). Of these materials, **3** contains a rare example of a $U^{VI}{-}U^{VI}$ cation–cation interaction. Coformation of all three phases is observed as a function of the reaction pH and is consistent with uranyl hydrolysis trends. Formation pathways were investigated using in situ Raman spectroscopy, the results of which are consistent with an increasingly diverse speciation portfolio at higher pH values.

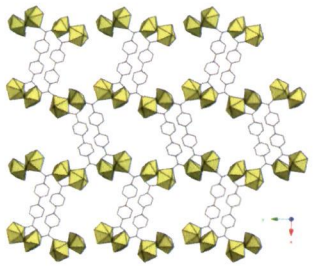

9496 S dx.doi.org/10.1021/ic401163y

Synthesis, Characterization, and Electron-Transfer Processes in Indium Ferrocenyl-Containing Porphyrins and Their Fullerene Adducts

Samantha J. Dammer, Pavlo V. Solntsev, Jared R. Sabin, and Victor N. Nemykin*

Three new indium(III) ferrocenyl-containing porphyrins have been prepared and characterized by spectroscopic methods. Structures of ClInTFcP, FcInTFcP, and FcInTFcP@$4C_{60}$ compounds have been reported. The redox properties of all new compounds were examined by electrochemical, spectroelectrochemical, and chemical oxidation methods. The electronic structure, energies of atropisomers, and the interaction of FcInTFcP with C_{60} were probed by DFT calculations.

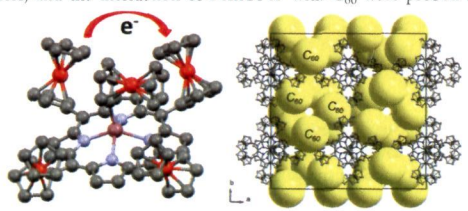

9511 S dx.doi.org/10.1021/ic4011746

Synthesis and Oxidative Reactivity of 2,2′-Pyridylpyrrolide Complexes of Ni(II)

Nikolay P. Tsvetkov, Chun-Hsing Chen, José G. Andino, Richard L. Lord, Maren Pink, René W. Buell, and Kenneth G. Caulton*

Synthesis and characterization of divalent nickel complexed by 2-pyridylpyrrolide bidentate ligands are reported, as possible precursors to complexes with redox active ligands. Varied substituents on the pyrrolide, two CF_3 (L^2), two ^{t}Bu (L^0), and one of each type (L^1) are employed and the resulting $Ni(L^n)_2$ complexes show different Lewis acidity toward CO, H_2O, THF or MeCN, the L^2 case being the most acidic.s

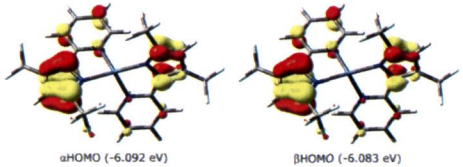

9522 S dx.doi.org/10.1021/ic401180r

Water Oxidation Catalysis with Nonheme Iron Complexes under Acidic and Basic Conditions: Homogeneous or Heterogeneous?

Dachao Hong, Sukanta Mandal, Yusuke Yamada, Yong-Min Lee, Wonwoo Nam,* Antoni Llobet,* and Shunichi Fukuzumi*

Water oxidation by Ce^{IV} was catalyzed by nonheme iron complexes under acidic conditions. The ligand of the iron complexes dissociated and oxidized to yield CO_2, resulting in limited reactivity. In contrast to the homogeneous catalysis under acidic conditions, light-driven water oxidation was catalyzed by iron hydroxide nanoparticles derived from the iron complexes as the result of the ligand dissociation under basic conditions.

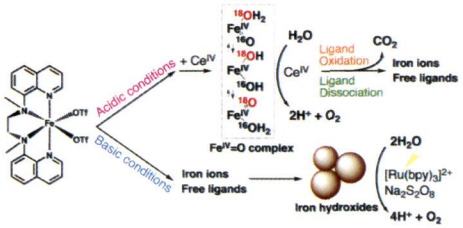

9532 S dx.doi.org/10.1021/ic401214e

Electrochemically Driven Intramolecular Oxidative Aromatic Coupling as a Pathway toward π-Extended Porphyrins

Ping Chen, Yuanyuan Fang, Karl M. Kadish,* Jan P. Lewtak, Dominik Koszelewski, Anita Janiga, and Daniel T. Gryko*

The electrochemical properties of *meso*-substituted and *meso*,*β*-fused naphthalene Ni porphyrins in nonaqueous media are reported. The exact order of steps in the electrochemical conversion of the naphthalene-substituted to the naphthalene-fused derivatives is investigated.

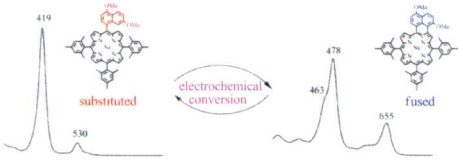

9539 S dx.doi.org/10.1021/ic401192x

Effects of Metal Coordination on the π-System of the 2,5-Bis-{(pyrrolidino)-methyl}-pyrrole Pincer Ligand

Christian Maaß, Diego M. Andrada, Ricardo A. Mata,* Regine Herbst-Irmer, and Dietmar Stalke*

Pincer complexes of 2,5-bis{(pyrrolidino)-methyl}-pyrrole with group 14 elements were prepared and characterized by X-ray single-crystal analysis, NMR spectroscopy, and mass spectrometry. Interaction with the pyrrole π-system was elaborated. Electronic structure calculations were carried out with group 14 complexes. The changes in the aromaticity of the pyrrole ring have been rationalized according to the interaction of the π-system. The short bond distance observed between germanium and the coordinated pyrrole nitrogen was assessed.

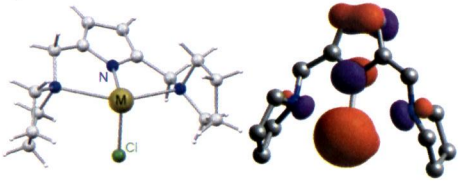

9549 S dx.doi.org/10.1021/ic401515q

Synthesis, Structure, and Reactivity of Lanthanide Complexes Incorporating Indolyl Ligands in Novel Hapticities

Zhijun Feng, Xiancui Zhu, Shaoyin Wang, Shaowu Wang,* Shuangliu Zhou, Yun Wei, Guangchao Zhang, Baojia Deng, and Xiaolong Mu

Reactions of 2-amino-functionalized indole with lanthanide amides led to discovery of different reactivity patterns and novel μ-η^6:η^1:η^1 bonding modes of indolyl ligands. The novel μ-η^6:η^1:η^1 bond modes can be converted to μ-η^3:η^1:η^1 or μ-η^2:η^r:η^1, depending on the steric effects of the formamidinato ligands and coordination of THF molecule.

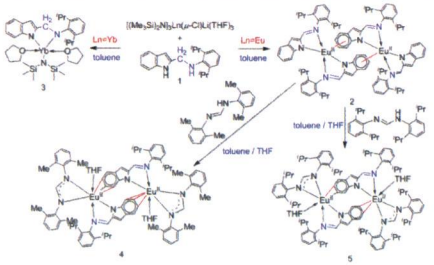

9557 S dx.doi.org/10.1021/ic401270j

Oxygen-Atom Transfer from Iodosylarene Adducts of a Manganese(IV) Salen Complex: Effect of Arenes and Anions on I(III) of the Coordinated Iodosylarene

Chunlan Wang, Takuya Kurahashi, Kensuke Inomata, Masahiko Hada, and Hiroshi Fujii*

We herein prepared iodosylarene adducts of a manganese(IV) salen complex from iodosylbenzene, iodosylmesitylene, 2,4,6-triethyliodosylbenzene, and pentafluoroiodosylbenzene. We also investigated the effect of anions on I(III) by using chloride, benzoate, and *p*-toluenesulfonate. The present study shows that these iodosylarene adducts are indeed active oxygen-atom-transfer reagents and that their reactivity and selectivity are regulated by steric and electronic properties of the arenes and anions on I(III) of the coordinated iodosylarenes.

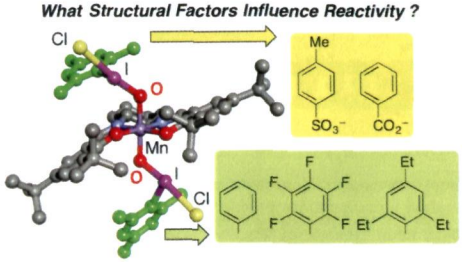

9567 dx.doi.org/10.1021/ic401276x

Inorganic Stressors of Ubiquitin

Giuseppe Arena, Francesco Bellia, Giuseppina Frasca, Giulia Grasso, Valeria Lanza, Enrico Rizzarelli, Giovanni Tabbi, Valeria Zito, and Danilo Milardi*

Metal-enriched, ubiquitin (Ub)-positive amyloid aggregates are a hallmark of neurodegeneration. Here we show that the anchoring of Cu^{II} and Zn^{II} ions to the His68 residue of Ub inhibits Lys48 and Lys63 self-polyubiquitination. These findings point to a close relationship between metal dyshomeostasis and malfunctioning of protein degradative pathways in age-related proteinopathies. *Metals misdrive ubiquitination.*

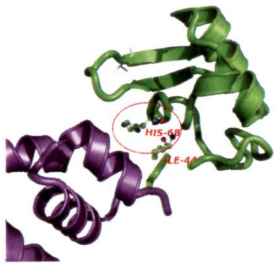

9574 S dx.doi.org/10.1021/ic401286a

Ligand Coordination and Spin Crossover in a Nickel Porphyrin Anchored to Mesoporous TiO_2 Thin Films

Darren Achey and Gerald J. Meyer*

The coordination and spin equilibrium of a Ni^{II} *meso*-tetra(4-carboxyphenyl)porphyrin compound, NiP, was quantified in fluid solution and when anchored to mesoporous nanocrystalline TiO_2 thin films. The semiconducting thin film was found to influence the kinetics and the thermodynamics for amine coordination to $Ni^{II}P$.

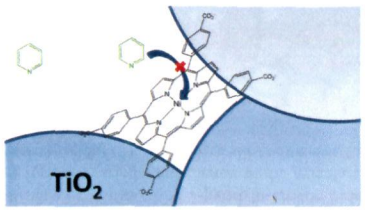

9583 S dx.doi.org/10.1021/ic4012873

Multimetallic Complexes Featuring a Bridging *N*-heterocyclic Phosphido/Phosphenium Ligand: Synthesis, Structure, and Theoretical Investigation

Baofei Pan, Deirdra A. Evers-McGregor, Mark W. Bezpalko, Bruce M. Foxman, and Christine M. Thomas*

By incorporating an N-heterocyclic phosphenium/phosphide (NHP) ligand into a chelating pincer ligand framework, we have elucidated several different and unprecedented binding modes of NHP ligands in homobimetallic, heterobimetallic, and *trimetallic metal complexes.*

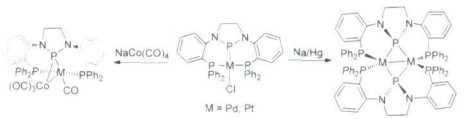

9590 S dx.doi.org/10.1021/ic401299h

A General Approach to Spindle-Assembled Lanthanide Borate Nanocrystals and Their Photoluminescence upon Eu^{3+}/Tb^{3+} Doping

Yubin Zeng, Zhengquan Li,* Yingfang Liang, Xiaoqin Gan, and Mengmeng Zheng

A series of spindle assemblies of $LnBO_3$ nanocrystals containing three kinds of crystalline phases have been developed, and their tunable luminescence is investigated after lanthanide doping.

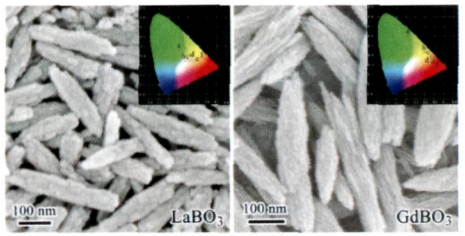

9597 S dx.doi.org/10.1021/ic4013203

Homo- and Heterometal Complexes of Oxido–Metal Ions with a Triangular [V(V)O–MO–V(V)O] [M = V(IV) and Re(V)] Core: Reporting Mixed-Oxidation Oxido–Vanadium(V/IV/V) Compounds with Valence Trapped Structures

Kisholoy Bhattacharya, Manoranjan Maity, Sk Md Towsif Abtab, Mithun Chandra Majee, and Muktimoy Chaudhury*

Trinuclear all-oxido–metal ion complexes with a V(V)O–MO–V(V)O triangular core [M = V(IV) and Re(V)] have been synthesized following a single-pot reaction protocol. The mixed-oxidation V(V)O–V(IV)O–V(V)O compounds (**1** and **2**) have trapped-valence structures as confirmed by single-crystal X-ray diffraction analysis, EPR and XPS spectroscopy, as well as BVS calculations.

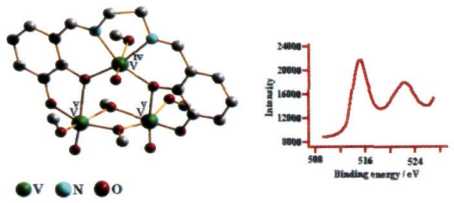

9606 dx.doi.org/10.1021/ic4013476

$CuCl_2$ for the Isolation of a Broad Array of Endohedral Fullerenes Containing Metallic, Metallic Carbide, Metallic Nitride, and Metallic Oxide Clusters, and Separation of Their Structural Isomers

Steven Stevenson* and Khristina A. Rottinger

Endohedral metallofullerenes with low 1st oxidation potentials can now be separated from other metallofullerenes and empty-cage fullerenes that have higher 1st oxidation potentials. $CuCl_2$ is discovered as the precipitating agent (Lewis acid) to selectively complex those endohedral species with low 1st oxidation potentials. Decomplexation of precipitated endohedrals is readily achieved with efficient recovery.

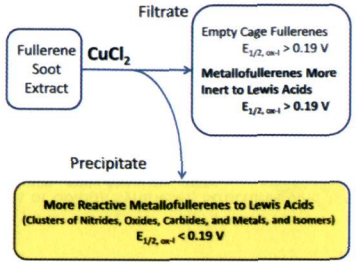

9613 dx.doi.org/10.1021/ic401314a

Synthesis and Isomerization of N-Fused Tetraphenylporphyrin Ruthenium(II) Complexes

Motoki Toganoh, Hideaki Matsuo, Ayumi Sato, Yuya Hirashima, and Hiroyuki Furuta*

Three possible isomers of N-fused tetraphenylporphyrin ruthenium complexes, $Ru(NFTPp)Cl(CO)_2$ (**2a–c**), were isolated and fully characterized by NMR, IR, CV, UV–vis-NIR absorption, and X-ray crystallography. Isomerization among **2a–c** occurred at elevated temperature through the intramolecular rotational pathways. Electronic structures of **2a–c** were analyzed by DFT study to reveal appreciable differences in the interaction between the NFTPp ligand and the Ru–Cl moiety.

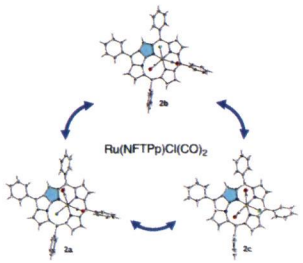

9620 dx.doi.org/10.1021/ic401378k

Dilution-Triggered SMM Behavior under Zero Field in a Luminescent Zn_2Dy_2 Tetranuclear Complex Incorporating Carbonato-Bridging Ligands Derived from Atmospheric CO_2 Fixation

Silvia Titos-Padilla, José Ruiz, Juan Manuel Herrera, Euan K. Brechin, Wolfgang Wersndorfer, Francesc Lloret, and Enrique Colacio*

The luminescent tetranuclear complex $\{(\mu_3\text{-}CO_3)\ [Zn(\mu\text{-}L)Dy(NO_3)]_2\}\cdot 4CH_3OH$ does not exhibit single-molecule magnet (SMM) behavior at zero applied direct-current field due to a fast quantum tunneling magnetization (QTM) relaxation process. However, a 1:10 Dy:Y dilute sample exhibits SMM behavior at $H_{dc} = 0$ with an important thermal energy barrier $U_{eff} = 68$ K. The paramagnetic to SMM transformation triggered only by dilution demonstrates the decisive role of the intermolecular dipolar interactions in favoring QTM relaxation.

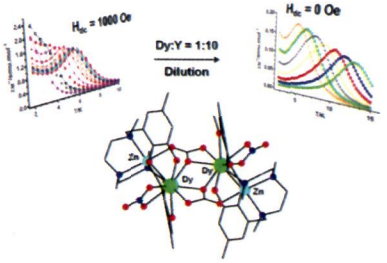

9627 dx.doi.org/10.1021/ic401408f

Magnetic Properties of the $RbMnPO_4$ Zeolite-ABW-Type Material: A Frustrated Zigzag Spin Chain

Gwilherm Nénert,* Jerry Bettis Jr., Reinhard Kremer, Hamdi Ben Yahia, Clemens Ritter, Etienne Gaudin, Olivier Isnard, and Myung-Hwan Whangbo

$RbMnPO_4$ is a rare example of a polar weak ferromagnet, exhibiting a Néel state below $T_N = 4.7$ K. In addition, this material shows magnetic frustration resulting in the emergence of an intermediate phase reminiscent of the multiferroic phase reported in $RMnO_3$. Theoretical analysis based on first-principles DFT calculations details the various magnetic exchange interactions that explain the observed complex behavior and ground state of the system.

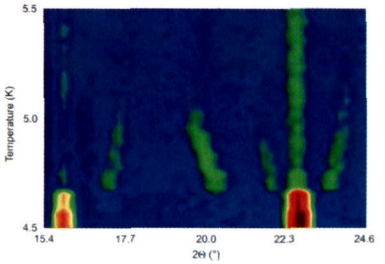

9636 S dx.doi.org/10.1021/ic401432m

Synthesis, Structures, and Dearomatization by Deprotonation of Iron Complexes Featuring Bipyridine-based PNN Pincer Ligands

Thomas Zell, Robert Langer, Mark A. Iron, Leonid Konstantinovski, Linda J. W. Shimon, Yael Diskin-Posner, Gregory Leitus, Ekambaram Balaraman, Yehoshoa Ben-David, and David Milstein*

Three phosphine-substituted pincer ligands, namely the known ^{t}*Bu-PNN (6-((di-tert-butylphosphino)methyl)-2,2′-bipyridine) and the two new* ^{i}*Pr-PNN (6-((di-iso-propylphosphino)methyl)-2,2′-bipyridine) and Ph-PNN (6-((diphenylphosphino)methyl)-2,2′-bipyridine) ligands, were synthesized and studied in ligation reactions with* FeX_2 (X = Cl, Br). *These reactions led to the formation of two types of complexes: mono-chelated neutral complexes* $[(R\text{-}PNN)Fe(X)_2]$ *and bis-chelated dicationic complexes* $[(R\text{-}PNN)_2Fe]^{2+}$. *Reactions of complexes* $[(R\text{-}PNN)_2Fe]^{2+}$ *with* KO^{t}Bu *give doubly deprotonated complexes* $[(R\text{-}PNN^*)_2Fe]$, *which have been studied in protonation reactions.*

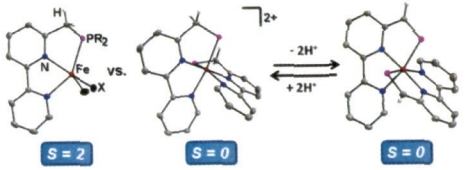

9650 S dx.doi.org/10.1021/ic401450u

Oxidation-Potential Tuning of Tungsten–Alkylidyne Complexes over a 2 V Range

Daniel E. Haines, Daniel C. O'Hanlon, Joseph Manna, Marya K. Jones, Sarah E. Shaner, Jibin Sun, and Michael D. Hopkins*

The oxidation potentials of d^2 tungsten–alkylidyne complexes of the form $W(CR)L_nL'_{4-n}X$ are tunable over a 2 V range *through ligand variation. The potentials are more sensitive* to the nature of the L ligands than to the CR and X ligands due to their different symmetry relationships to the d_{xy} redox orbital. The HOMO energy and oxidation potential are linearly related, consistent with the reorganization energy for oxidation being small.

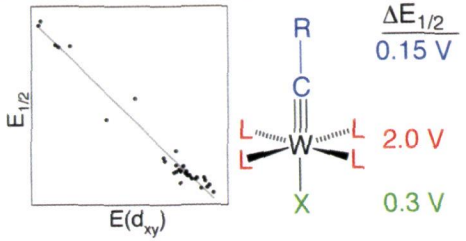

9659 S dx.doi.org/10.1021/ic4014569

Azido, Triazolyl, and Alkynyl Complexes of Gold(I): Syntheses, Structures, and Ligand Effects

Thomas J. Robilotto, Nihal Deligonul, James B. Updegraff III, and Thomas G. Gray*

[3 + 2] Cycloadditions of gold(I) azides and terminal alkynyls yield (triazolyl)gold(I) complexes.Gold(I) azides, triazolyls, and alkynyls are described.

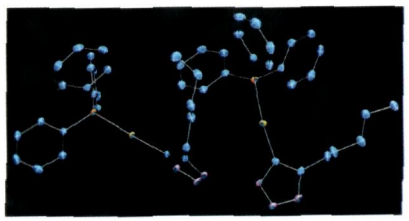

9669 dx.doi.org/10.1021/ic4014762

Tracing Hydrogen Bonding Au···H–C at Gold Atoms: A Case Study

Florian Kraus,* Hubert Schmidbaur,* and Salih S. Al-juaid

A DFT investigation of the structures of three cyclometalated 6-benzylpyridines with gold(III) centers in the metallacycle have shown that the reported close transannular Au···H–C contacts are not associated with a significant attractive interaction.

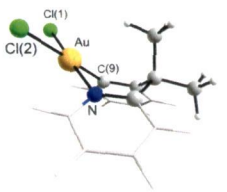

9675 S dx.doi.org/10.1021/ic401492q

New {RuNO} Polyoxometalate $[PW_{11}O_{39}Ru^{II}(NO)]^{4-}$: Synthesis and Reactivity

Maxim N. Sokolov,* Sergey A. Adonin, Dmitry A. Mainichev, Pavel L. Sinkevich, C. Vicent, Nikolay B. Kompankov, Artem L. Gushchin, V.A. Nadolinny, and Vladimir P. Fedin

New Ru-substituted Keggin-type polyoxometalate complex containing nitroso ligand, $[PW_{11}O_{39}Ru(NO)]^{4+}$, has been prepared. *It is converted by hydrazin or* hydroxylamine into aqua complex $[PW_{11}O_{39}Ru^{III}(H_2O)]^{4+}$ in quantitative yield. Intermediate complex of dinitrogen has been detected. Sn^{2+} converts $[PW_{11}O_{39}Ru(NO)]^{4+}$ *into* $[PW_{11}O_{39}Ru(NH_3)]^{4+}$.

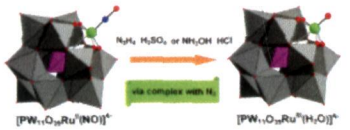

9683 S dx.doi.org/10.1021/ic401555g

Hydrogen Bonding and Electron Transfer between Dimetal Paddlewheel Compounds Containing Pendant 2-Pyridone Functional Groups

Luke A. Wilkinson, Laura McNeill, Paul A. Scattergood, and Nathan J. Patmore*

A series of quadruply bonded dimetal paddlewheel compounds containing 1, 2, or 4 pendant 2-pyridone functional groups has been synthesized. Self-complementary hydrogen bonding is observed in dichloromethane for compounds with a single pendant hydrogen bond donor/acceptor, resulting in the formation of "dimers of dimers". Electron transfer through these hydrogen bonded assemblies was investigated using cyclic voltammetry.

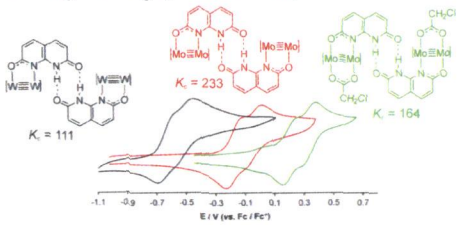

dx.doi.org/10.1021/ic4016838

Synthesis and Structure of Perovskite $ScMnO_3$

Haiyan Chen, Tian Yu, Peng Gao, Jianming Bai, Jing Tao, Trevor A. Tyson,* Liping Wang, and Roger Lalancette

Metastable small R-ion $RMnO_3$ perovskites possess intriguing electronically driven electrical polarization, but the synthesis of the perovskite phase for the end member $ScMnO_3$ system has proven to be elusive. We report the structure of a new monoclinic $P2_1/n$ perovskite phase of $ScMnO_3$ synthesized from the hexagonal phase under high-pressure and high-temperature conditions. This extends the small ion region for so-called E-phase electronically driven ferroelectric manganese perovsites possibly leading to a better understanding of these materials.

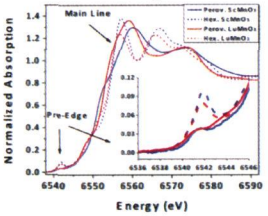

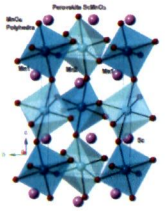

Supporting Information available via online article